Elastodynamically Induced Spin and Charge Pumping in Bulk Heavy Metals

Farzad Mahfouzi* and Nicholas Kioussis†
Department of Physics and Astronomy, California State University Northridge, Northridge, California 91330-8268, USA

(Received 11 October 2021; revised 11 April 2022; accepted 10 May 2022; published 27 May 2022)

Analogous to the spin-Hall effect (SHE), *ab initio* electronic structure calculations reveal that acoustic phonons can induce charge (spin) current flowing along (normal to) its propagation direction. Using the Floquet approach we have calculated the elastodynamically induced charge and spin pumping in bulk Pt and demonstrate that (i) the longitudinal charge pumping originates from the Berry curvature, while the transverse pumped spin current is an odd function of the electronic relaxation time and diverges in the clean limit. (ii) The longitudinal charge current is of nonrelativstic origin, while the transverse spin current is a relativistic effect that to lowest order scales linearly with the spin-orbit coupling strength. (iii) Both charge and spin pumped currents have parabolic dependence on the amplitude of the elastic wave.

DOI: 10.1103/PhysRevLett.128.215902

Introduction.—One of the primary objectives in the field of spintronics is the development of efficient means to generate pure spin current, which can be in turn used to manipulate the magnetization configuration and damping rate in magnetic based memory bits [1], spin transistors [2,3], antennas [4], and sensors [5]. Generating spin current in materials with strong spin-orbit coupling (SOC) through the spin Hall effect [6] (SHE), i.e., the transverse spin current generation by electric field, has recently been the focus of intensive research both theoretically and experimentally [7,8]. The SHE is often parametrized by the charge-to-spin current conversion efficiency, referred to as the spin-Hall angle, Θ_{SH}, whereby the spin current is given by $\vec{I}_{\vec{s}} = (\hbar/2e)\Theta_{\mathrm{SH}}\vec{I}_C \times \vec{e}_{\vec{s}}$. Here, $\vec{e}_{\vec{s}}$ is the spin polarization unit vector and $\vec{I}_C$ is the charge current. Experimentally, the conventional approach to quantify Θ_{SH} is through spin-orbit torque measurements in ferromagnetic–normal-metal bilayer devices [9–15].

Another commonly used mechanism to generate dc spin current is the spin pumping from a precessing ferromagnet (FM) into an adjacent normal metal (NM) [16–20]. The generated spin current flowing through the FM/NM interface is $I_{\vec{s}} = (\hbar/4\pi)g_{\uparrow\downarrow}\vec{e}_{\vec{s}} \cdot \vec{m} \times \partial\vec{m}/\partial t$, where $\vec{m}$ and $g_{\uparrow\downarrow}$ denote the direction of the magnetization and the spin-mixing conductance, respectively. $g_{\uparrow\downarrow}$ is often determined experimentally through the change of Gilbert damping in the presence and absence of the normal metal adjacent to the FM [21]. In addition, other approaches, such as the spin polarization effect in magnetic tunnel junctions [22,23], the spin Seebeck effect [24–27], spin pumping from magnons excited in response to elastic waves [28,29], and spin current pulses produced by the ultrafast laser induced demagnetization process [30,31] have also been proven to be promising for the generation of spin currents in spintronic devices.

Recently, a different approach to generate spin current was demonstrated experimentally in X/CoFeB/MgO ($X = \mathrm{W}, \mathrm{Pt}, \mathrm{W}$) heterostructures where the spin current emerges from the lattice dynamics in strong spin-orbit nonmagnetic metals (Pt, W), and flows transverse to the propagation direction of the surface acoustic wave [32]. This is similar to the conventional SHE where the spin current propagates orthogonal to the electrical current. To account for the experimental results Kawada *et al.* suggested [32] that the spin current must scale with the SOC and the time derivative of the lattice displacement along the wave propagation direction. The suggested plausible mechanisms of the generation of acoustic spin Hall effect include a dynamic change in the Berry curvature of electron wave function induced by the time-dependent lattice displacement giving rise to a Berry electric field [33,34], and/or SOC-mediated spin-lattice coupling resembling the Rashba Hamiltonian [35]. Nevertheless, the underlying atomistic mechanism remains unresolved.

In this Letter, using *ab initio* based electronic structure calculations we reveal the emergence of a dc charge (spin) current in response to acoustic phonons in heavy metals (Pt), shown schematically in Fig. 1(a), where the spin current flows transverse to the phonon propagation direction. We demonstrate that the phonon-induced spin current is a relativistic effect arising from the SOC where, to the lowest order, depends linearly on the SOC strength. Analogous to the SHE, the spin polarization orientation is orthogonal to both the spin current and phonon propagation directions. We show that the phonon-induced charge (spin) current saturates (diverges) in the limit of ballistic transport regime. This is in sharp contrast to the electric field-induced charge (spin) current where the corresponding longitudinal (transverse) conductivity saturates (diverges) in the clean system limit.

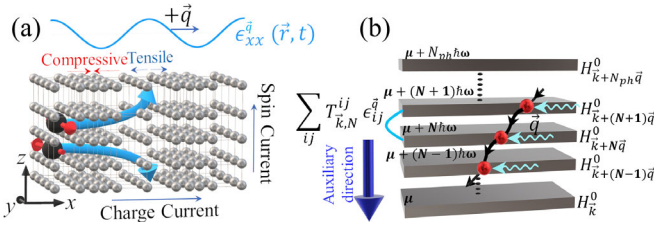

FIG. 1. (a) Schematic of the elastodynamically induced charge and spin current in bulk heavy metal under a time- and position-dependent strain $\epsilon_{xx}(\vec{R},t) = \mathrm{Re}(\epsilon_{xx}^{\vec{q}} e^{i\omega t + i\vec{q}\cdot\vec{R}})$, of wave vector $\vec{q}$ along the x direction. The charge current propagates along $\vec{q}$, while the spin current flows (along z) orthogonal to the phonon and spin-polarization (y) directions. (b) Floquet space representation of the combined electron-phonon system. The phononic part consists of a single mode with wave vector $\vec{q}$ and a cutoff number, N_{ph}, of phonons. The Nth layer represents the electronic system with Hamiltonian $H^0_{\vec{k}+N\vec{q}}$ and chemical potential $\mu + N\hbar\omega$ that is coupled to the other electronic systems with different number of phonons through the electron-phonon coupling matrix, $T^{ij}_{\vec{k},N}$, $i, j = x, y$, and z.

Theoretical formalism.—In the linear response regime the electronic Hamiltonian of a bulk system under a time- and position-dependent strain, $\epsilon_{ij}(\vec{R},t)$ $(i,j = x,y,z)$, is given by [36,37]

$$\hat{\mathbf{H}} = \hat{\mathbf{H}}^0 + \frac{1}{2}\sum_{ij}[\hat{\mathbf{H}}^{ij}\hat{\boldsymbol{\epsilon}}_{ij}(t) + \hat{\boldsymbol{\epsilon}}_{ij}(t)\hat{\mathbf{H}}^{ij}]. \tag{1}$$

Here, bold symbols denote matrices in real space, hat symbols denote matrices in atomic orbital Hilbert space, $\hat{\mathbf{H}}^0$ is the Hamiltonian in the absence of strain, $\hat{\mathbf{H}}^{ij} = \partial\hat{\mathbf{H}}/\partial\epsilon_{ij}|_{\epsilon_{ij}\to 0}$ is the deformation Hamiltonian term associated with the coupling between electrons and local strain, $[\hat{\mathbf{H}}]_{\vec{R},\vec{R}'} = \hat{H}_{\vec{R}-\vec{R}'}$, $\vec{R}, \vec{R}'$ are the positions of the unit cells, and the time- and position-dependent local strain is a diagonal matrix with elements given by $[\hat{\boldsymbol{\epsilon}}_{ij}]_{\vec{R},\vec{R}'} = \hat{1}\epsilon_{ij}(\vec{R},t)\delta_{\vec{R},\vec{R}'}$. Equation (1) assumes that spatial variation of strain is adiabatic and hence ignores the dependence of the Hamiltonian on the gradience of strain. For a single phonon mode of wave vector $\vec{q}$ and frequency ω we have $\epsilon_{ij}(\vec{R},t) = \mathrm{Re}(\epsilon_{ij}^{\vec{q}} e^{i\omega t + i\vec{q}\cdot\vec{R}})$. In this case, the time and position dependence of the Hamiltonian can be removed by applying a gauge transformation, $[\hat{\mathbf{U}}]_{NM} = \delta_{NM}\hat{1}e^{iN\omega t + iN\vec{q}\cdot\vec{R}}$, where the capital letters, N and M refer to phonon states. The resulting time-independent system is referred to as the Floquet space, where the corresponding Hilbert space is extended to include the phononic degrees of freedom, with the total Hamiltonian given by

$$[\hat{\mathcal{H}}_{\vec{k}}]_{NM} = \hat{H}^0_{\vec{k}+N\vec{q}}\delta_{NM} + \frac{1}{2}\sum_{ij}\hat{T}^{ij}_{\vec{k},N}\epsilon^{\vec{q}}_{ij}(\delta_{N,M+1} + \delta_{N,M-1}), \tag{2}$$

where $\hat{T}^{ij}_{\vec{k},N} = \frac{1}{2}(\hat{H}^{ij}_{\vec{k}+N\vec{q}} + \hat{H}^{ij}_{\vec{k}+(N+1)\vec{q}})$, $N, M = 0, \ldots, N_{\mathrm{ph}}$, and N_{ph} is the cutoff for the number of phonons. The hybrid electron-phonon Hamiltonian is shown schematically in Fig. 1(b), where the additional dimension is introduced to account for the single mode phononic degree of freedom. The dependence of the quasiparticle chemical potential on the number of phonons results in a quasiparticle transport along the auxiliary direction which describes the attenuation of the single mode elastic wave through electron-phonon scattering [38]. In this case, due to the conservation of momentum, both electrons and holes are dragged along the phonon propagation direction, whereby systems with electron-hole asymmetry experience a net pumped charge current. This mechanism of pumping is, in essence, similar to the phonon drag effect that gives rise to an enhancement of Seebeck coefficient which is often treated theoretically using coupled electron-phonon Boltzmann transport equations [39].

For an isolated system, the wave function of the coupled electron-phonon system is of the form $|N\alpha\vec{k}\rangle = |N\rangle \otimes |\alpha\vec{k}\rangle$, where, $\otimes$ refers to the Kronecker product, and α denotes the atomic orbitals and spin of the electron Bloch states. The single quasiparticle retarded Green's function and the corresponding density matrix can be obtained from [38,40]

$$\hat{\boldsymbol{\rho}}_{\vec{k}} = \frac{\eta}{\pi}\int dE\hat{\mathbf{G}}_{\vec{k}}(E)f(E\hat{\mathbf{1}} - \hat{\boldsymbol{\Omega}})\hat{\mathbf{G}}^{\dagger}_{\vec{k}}(E), \tag{3}$$

where the Green's function is calculated from

$$(E - i\eta - \hat{\boldsymbol{\mathcal{H}}}_{\vec{k}} - \hat{\boldsymbol{\Omega}})\hat{\mathbf{G}}_{\vec{k}}(E) = \hat{\mathbf{1}}. \tag{4}$$

Here, $[\hat{\boldsymbol{\Omega}}]_{NM} = N\hbar\omega\delta_{NM}\hat{1}$, is the single mode phononic Hamiltonian, $f(E)$ is the Fermi-Dirac distribution function and $\eta = \hbar/2\tau$ is the energy broadening parameter which is inversely proportional to the electronic relaxation time τ. Using the density matrix given by Eq. (4), the charge and spin currents are determined from,

$$\vec{I} = e\langle\vec{\hat{\mathbf{v}}}_{\vec{k}}\rangle, \tag{5a}$$

$$\vec{I}^{S_i} = \frac{\hbar}{2}\mathrm{Re}\langle\hat{\sigma}_i\vec{\hat{\mathbf{v}}}_{\vec{k}}\rangle, \tag{5b}$$

where, $\langle\ldots\rangle = \sum_{\vec{k}}\mathrm{Tr}[\ldots\hat{\boldsymbol{\rho}}_{\vec{k}}]/(VN_kN_{\mathrm{ph}})$ is the expectation value, V is the volume of the unit cell, N_k is the number of k points in the summation and $\vec{\hat{\mathbf{v}}}_{\vec{k}} = \partial\hat{\mathcal{H}}_{\vec{k}}/\partial\vec{k}$ is the electronic group velocity operator. In the ballistic regime and in linear response to the phonon frequency, ω, the density matrix is given by

$$\hat{\boldsymbol{\rho}}_{\vec{k}} \approx f(\hat{\mathcal{H}}_{\vec{k}} + \hat{\boldsymbol{\Omega}}) + \frac{\eta}{\pi}\hat{\mathbf{G}}_{\vec{k}}(E_F)\hat{\boldsymbol{\Omega}}\hat{\mathbf{G}}^{\dagger}_{\vec{k}}(E_F). \tag{6}$$

The first and second terms in Eq. (6) are referred to as the Fermi sea and Fermi surface contributions, respectively.

The Fermi surface contribution to the density matrix and the resulting pumped charge and spin currents can be separated into even and odd components with respect to η (or relaxation time), $\hat{\boldsymbol{\rho}}_{\vec{k}}^{\text{even/odd}} = [\hat{\boldsymbol{\rho}}_{\vec{k}}(\eta) \pm \hat{\boldsymbol{\rho}}_{\vec{k}}(-\eta)]/2$. To lowest order, the even (odd) component is expected to be independent of (inversely proportional to) η, demonstrating its Berry- (Ohmic-)like character (see Supplemental Material [41]).

The Berry curvature nature of the even component of the charge current can be further demonstrated by rewriting the charge pumping expression as the Berry curvature in mixed time-k space (see Supplemental Material [41])

$$\vec{I}^{\text{even}} = \frac{2e}{VN_kN_{\text{ph}}}\sum_{n\vec{k}} f(\varepsilon_{n\vec{k}})\text{Im}\left\langle \frac{\partial\psi_{n\vec{k}}}{\partial\vec{k}}\middle|\hat{\boldsymbol{U}}^{\dagger}\frac{\partial}{\partial t}\hat{\boldsymbol{U}}\middle|\psi_{n\vec{k}}\right\rangle = \frac{2e}{VN_kN_{\text{ph}}}\sum_{n\vec{k}} f(\varepsilon_{n\vec{k}})\text{Re}\left\langle \frac{\partial\psi_{n\vec{k}}}{\partial\vec{k}}\middle|\hat{\boldsymbol{\Omega}}\middle|\psi_{n\vec{k}}\right\rangle, \tag{7}$$

where, we use perturbation theory to express, $|\partial\psi_{n\vec{k}}/\partial\vec{k}\rangle = \sum_m(\vec{\hat{\boldsymbol{v}}})_{nm}|\psi_{m\vec{k}}\rangle/(\varepsilon_{n\vec{k}}-\varepsilon_{m\vec{k}}-i\eta)$, with $\vec{\hat{\boldsymbol{v}}}_{nm,\vec{k}} = \langle\psi_{n\vec{k}}|\vec{\hat{\boldsymbol{v}}}|\psi_{m\vec{k}}\rangle$ being the group velocity matrix elements, and the energy broadening parameter, η, is introduced to avoid divergences at the degenerate points. The wave function, $|\psi_{n\vec{k}}\rangle$ and energy dispersion, $\varepsilon_{n\vec{k}}$ are the eigenvectors and eigenvalues of the Floquet Hamiltonian, $\hat{\boldsymbol{\mathcal{H}}}_{\vec{k}}$, respectively. The Berry curvature(even) component of the pumped spin current can be calculated from an expression similar to Eq. (7), by replacing the charge current operator $e\vec{\hat{\boldsymbol{v}}}$ with the spin current operator given by the Hermitian part of $\hbar\hat{\sigma}_i\vec{\hat{\boldsymbol{v}}}/2$. Furthermore, it should be noted that in systems with small band gap at the Fermi surface, the topological nature of Eq. (7) can yield quantized values (i.e., independent of elastic wave amplitude), where electrons and holes are trapped and dragged by the elastic wave, resulting in the so-called Thouless pumping [42,44].

Computational approach.—The tight-binding Hamiltonian $\hat{H}_{\vec{k}}$ matrices for bulk Pt under different values of strain, ϵ_{ij}, are calculated using the linear combination of atomic orbitals OpenMX package [45–47]. For a nonmagnetic material, the one-electron Kohn-Sham Hamiltonian can be expressed by [38,48,49]

$$\hat{H}_{\vec{k}}(\{\epsilon_{ij}\}) = \hat{H}^{K}_{\vec{k}}(\{\epsilon_{ij}\})\hat{1}_{2\times2} + \xi\hat{H}^{\text{soc}}_{\vec{k}}(\{\epsilon_{ij}\}), \tag{8}$$

where, the first term represents the kinetic component of the Hamiltonian, the second term is the SOC contribution, and ξ is the corresponding scaling factor. The effect of strain ϵ_{ij} is to modify the primitive lattice vectors $\vec{a}_i'$ such that $(\vec{a}_i' - \vec{a}_i)\cdot\vec{e}_j = \sum_k \vec{a}_i\cdot\vec{e}_k\epsilon_{kj}$, where the $\vec{e}_j$'s denote unit vectors in Cartesian coordinates. The electron-phonon coupling terms in Eq. (1) are calculated by fitting Eq. (8) to a polynomial function, and in turn calculate $\hat{H}^{ij}_{\vec{k}} = \partial\hat{H}_{\vec{k}}/\partial\epsilon_{ij}|_{\epsilon_{ij}\to0}$. The self-consistent (SCF) calculations employ the Troullier-Martins type norm-conserving pseudopotentials [50] with partial core correction. The equilibrium lattice constant of bulk Pt was set to $a = 3.96$ Å. In the SCF calculations we used a 24^3 k-point mesh in the first Brillouin zone, and an energy cutoff of 350 Ry for numerical integrations in the real space grid. For the exchange correlation functional the LSDA [51] parametrized by Perdew and Wang [52] was used.

TABLE I. Values of the even and odd contributions to the elastodynamical-induced components of the pumped charge $\vec{I}$, and spin current $\vec{I}^{S_i}$, divided by the acoustic phonon frequency ω, (in units of $10^{10}/e\Omega m^2$), for phonon wave vector $\vec{q} = (\pm0.01, 0, 0)(\text{Å}^{-1})$ and strain amplitude $\epsilon_{xx}^{\vec{q}} = 10^{-3}$.

	Even			Odd		
$i =$	x	y	z	x	y	z
$I_i(\vec{q})/\omega$	±80	0	0	0	0	0
$I_i^{S_x}(\vec{q})/\omega$	0	0	0	0	0	0
$I_i^{S_y}(\vec{q})/\omega$	0	0	0	0	0	∓0.7
$I_i^{S_z}(\vec{q})/\omega$	0	0	0	0	±0.7	0

Results and discussion.—Table I lists the values of the even and odd contributions to the elastodynamically induced components of the pumped charge, $\vec{I}$, and spin current, $\vec{I}^{S_i}$, divided by the acoustic phonon frequency ω (in units of $10^{10}/e\Omega m^2$), for $\vec{q} = (\pm0.01, 0, 0)(\text{Å}^{-1})$, strain amplitude $\epsilon_{xx}^{\vec{q}} = 10^{-3}$ and $\eta = 0.01$ eV. The charge current is an even function of η and is parallel to the elastic wave propagation direction $\vec{I}\|\vec{q}$ while the spin current is an odd function of η and propagates normal to $\vec{q}$ and the spin polarization direction, $\vec{I}^{\vec{S}}\|\vec{e}_{\vec{S}}\times\vec{q}$. Figure 2(a) displays the calculated pumped charge (dashed curve) and spin (solid curve) currents versus the wave vector of the elastic wave propagating along x, respectively, with $\epsilon_{xx}^{\vec{q}} = 10^{-3}$ and $\eta = 0.01$ eV. Both charge and spin currents are odd functions of the wave vector with a linear dependence on q_x close to the Γ point. This is analogous to the electric field-induced charge and spin current, where the external electric field is replaced with $\hbar\omega\vec{q}/e$. The difference, however, is that in contrast to the Ohmic (spin-Hall) currents that are odd (even) functions of the relaxation time, the phonon-induced charge (spin) current exhibits even (odd) dependence on η.

The slope of the pumped charge and spin currents with respect to q_x in the limit of $q_x \to 0$, describes the efficiency of the phonon-induced electronic transport in the material. Hence, in Fig. 2(b) we show the variation of the elastodynamically induced charge current $I_x^{\text{even}}/q_x\omega$ and the spin current $I_z^{S_y;\text{odd}}/q_x\omega$ versus $(\epsilon_{xx}^{\vec{q}})^2$. The calculations reveal that both the charge (dashed curve) and the spin current

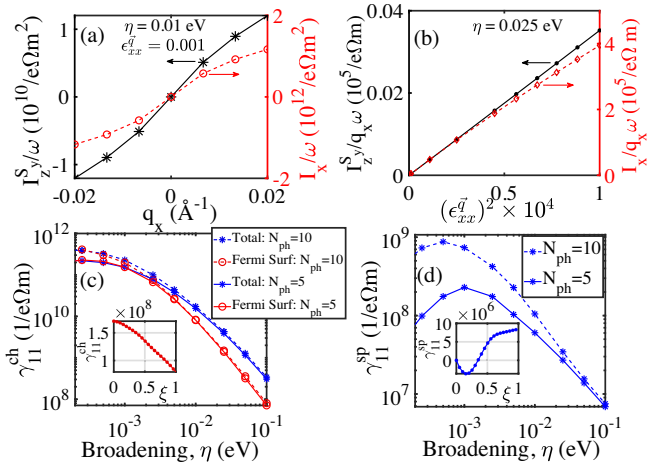

FIG. 2. (a) Elastodynamical pumped spin (left-hand ordinate) and charge (right-hand ordinate) current divided by the phonon frequency ω versus the phonon wave vector $\vec{q}$ along the x axis with strain amplitude $\epsilon^{\vec{q}}_{xx} = 10^{-3}$ and energy broadening parameter $\eta = 10$ meV. (b) Efficiency of the elastodynamically induced spin current, $I_z^{\mathrm{Sy;odd}}/q_x\omega$, (left-hand ordinate) and charge current, $I_x^{\mathrm{even}}/q_x\omega$, (right-hand ordinate) in the limit $q_x \to 0$, versus the square of the strain amplitude, $(\epsilon^{\vec{q}})^2_{xx}$, where $\epsilon^{\vec{q}}_{xx}$ ranges between 0% and 1%. (c) Total (stars) and Fermi surface (circles) contributions to the ELCC versus η for $N_{\mathrm{ph}} = 5$ and 10 shown with solid and dashed curves, respectively. (d) Fermi surface contribution to the ETSC versus η for different values of N_{ph}. Insets in (c) and (d): ELCC and ETSC versus SOC scaling factor for $\eta = 0.1$ eV.

(solid curve) vary quadratically with the amplitude of the elastic wave for a wide range of strain. These results suggest that the strain dependence of the elastodynamically induced pumped charge and spin currents can be written in the general form,

$$\vec{I}(\vec{q})/\omega = \vec{q} \sum_{i\le j,k\le l} \gamma^{ch}_{ij,kl}\epsilon^{\vec{q}}_{ij}\epsilon^{\vec{q}}_{kl}, \tag{9a}$$

$$\vec{I}^{\vec{S}}(\vec{q})/\omega = \frac{\hbar}{2e}\vec{e}_{\vec{S}} \times \vec{q} \sum_{i\le j,k\le l} \gamma^{sp}_{ij,kl}\epsilon^{\vec{q}}_{ij}\epsilon^{\vec{q}}_{kl}, \tag{9b}$$

where, $\gamma^{ch}_{ij,kl}$ and $\gamma^{sp}_{ij,kl}$ are the elastodynamical longitudinal charge conductivity (ELCC) and elastodynamical transverse spin conductivity (ETSC), respectively. Given, $\epsilon_{ij} = \epsilon_{ji}$, in order to avoid double counting we consider only strains with $i \le j$. One can then use the Voigt notation ($[1, 2, 3, 4, 5, 6] \equiv [xx, yy, zz, yz, xz, xy]$) to represent the $\gamma^{ch/sp}_{ij,kl}$ tensor elements as a 6×6 symmetric matrix.

The variation of the ELCC versus the broadening energy η is shown in Fig. 2(c) for phonon cutoff number, $N_{\mathrm{ph}} = 5$ and 10. We display the variation of the total ELCC and its Fermi surface contribution, where the former is determined from Eq. (7), while the latter is calculated from Eq. (5) where the density matrix is given only by the second term in Eq. (6). We find that in the limit of the ballistic regime ($\eta \to 0$), the ELCC saturates to a finite value. On the other hand, in the limit of large η (diffusive regime), while the ELCC becomes independent of N_{ph}, the deviation between the total and Fermi surface contribution becomes more significant, due to the fact that Eq. (7) is derived and hence valid in the small η limit. The inset in Fig. 2(c) shows the dependence of ELCC on the SOC scaling factor with a finite value in the absence of SOC, demonstrating its nonrelativistic nature.

Figure 2(d) shows the variation of the odd component of ETSC (only the Fermi surface contribution) versus η for $N_{\mathrm{ph}} = 5$ and 10. In contrast to the expected $1/\eta$ dependence, we find that in the limit of $\eta \to 0$ the ETSC is proportional to η and reaches a peak with increasing η. The peak ETSC value increases with N_{ph}, and the corresponding $\eta_{\max}$ decreases with increasing N_{ph}, suggesting that ETSC $\propto \eta/(N_{\mathrm{ph}}^{-1} + c\eta^2)$, where c is a constant. This means, a larger phonon cutoff number is required to converge the ETSC value in the clean limit (small η limit). The inset in Fig. 2(d) shows the ETSC versus the SOC scaling factor ξ demonstrating its relativistic nature, which, analogous to the SHE, to lowest order in ξ, is proportional to the SOC strength. It is worth noting that the nonmonotonic dependence of ETSC and its sign reversal with SOC for small η suggests that in heavy metals (with large SOC) such as Pt a perturbative treatment of ETSC with respect to SOC may fail. Interestingly, the results of ETSC versus SOC shown in Fig. S1 in the Supplemental Material [41] for larger η of 0.5 eV exhibits a monotonic behavior.

Thus far, we have focused only on the elastodynamically induced pumping in response to a longitudinal elastic wave, $\epsilon_{xx}(\vec{R}, t)$. In the following we present the results for the nonzero matrix elements of the 6×6 elastodynamical charge or spin conductivity matrix. The values of the diagonal matrix elements for the even component of the ELCC matrix (in units of $10^9/e\Omega m$) for $\vec{q}\|x$ and $\eta = 25$ meV, are $\gamma^{ch}_{ii} = [1.5, 2.5, 2.5, 0.8, 1, 1]$, ($i = 1, \ldots, 6$), while those of the off-diagonal matrix elements are $\gamma^{ch}_{12} = \gamma^{ch}_{13} = -0.6$, and $\gamma^{ch}_{23} = -2.4$, where $\gamma^{ch/sp}_{ij} = \gamma^{ch/sp}_{ji}$. Note that similar to the elastic stiffness and magnetoelastic tensor elements [53], the symmetry of the crystal structure for the elastodynamical electronic transport reduces the number of independent tensor elements. However, the difference is that the elastic wave propagation along the x axis breaks the cubic symmetry and the ELCC matrix elements resemble those of a tetragonal system instead.

Similar calculations for the ETSC (in units of $10^7/e\Omega m$) with spin current along the z axis and spin polarization along the y axis, yields that the nonzero diagonal elements are $\gamma^{sp}_{ii} = [3.5, 2.6, -0.6, 2, 0.5, -0.4]$ and the off-diagonal elements are $\gamma^{sp}_{12} = -3.3$, $\gamma^{sp}_{13} = -1.6$, and $\gamma^{sp}_{23} = 1.6$.

Note that all of the nonzero elements of ETSC are independent, similar to the elastic stiffness matrix elements of an orthorhombic crystal structure. This is due to the fact that the choice of the spin current direction along z renders the yz plane (i.e., normal to $\vec{q}\|\vec{e}_x$) anisotropic.

As demonstrated in the Supplemental Material [41], the underlying mechanism of the phonon-induced pumping can be attributed to the electron-hole asymmetry, which results in a negative (positive) sign for ELCC when the transport is electron-(hole-)like. The derivative of density of states (DOS) with respect to the energy can be employed to qualitatively determine the sign of the phonon-induced charge pumping. We find a correlation between ELCC, ETSC and the derivative of DOS as a function of chemical potential shift (see Fig. S2 in Ref. [41]), suggesting that the ETSC may be explained by the phonon drag charge current combined with the spin-Hall effect.

An approximate value of the experimental ELCC can be determined from $\vec{I} \approx \omega \vec{q} \gamma_{\mathrm{eff}}^{ch} \epsilon_{\mathrm{eff}}^2$, using the measured values [32] of pumped charge current, $I = 7.5 \times 10^3\ (\mathrm{A/m^2})$, in response to an elastic wave with frequency $\nu = 193$ MHz, wavelength, $\lambda = 20\ \mu$m, and strain amplitude $\epsilon_{\mathrm{eff}} \approx 0.01\%$ [54]. An effective value of ELCC, $\gamma_{\mathrm{eff}}^{ch,\mathrm{exp}} \approx 10^{12}\ (1/e\Omega m)$ is then estimated, which is near the upper limit of the theoretical value in Fig. 2(c), corresponding to the clean limit, $\eta \to 0$. A more accurate comparison with experiment requires taking into account all ELCC tensor elements. Moreover, the spin current calculated in this work accounts only for the conventional bulk component and neglects the spin torque [55,56] and the FM/NM interfacial [48] contributions that are both quadratic in SOC and are higher-order corrections to the conventional SHE [57]. Therefore, a proper comparison with experiment requires calculations of the elastodynamical spin orbit torque in bilayer systems. It should also be noted that the relaxation time approximation is reliable only in the small η limit, since the limit of large η violates conservation laws, resulting in a smaller pumped spin current [38,58].

In conclusion, we have developed a Floquet-based approach using density functional theory and demonstrated the emergence of charge and spin currents induced by an acoustic phonon in bulk Pt. The calculations unveil the underlying atomistic mechanism of the recently discovered acoustic spin Hall effect in strong spin-orbit metals [32]. We find that the pumped charge (spin) current flows along (normal to) the phonon wave vector, and is of nonrelativistic (relativistic) origin. It is worth mentioning that the phonon-induced pumped charge and spin current effect presented in this Letter can be generalized to other bosonic excitations (e.g., magnons, photons, etc.) and their combinations.

The authors are grateful for fruitful discussions with Masamitsu Hayashi and Takuya Kawada. The work is supported by NSF ERC-Translational Applications of Nanoscale Multiferroic Systems (TANMS)- Grant No. 1160504, NSF PFI-RP Grant No. 1919109, and by NSF-Partnership in Research and Education in Materials (PREM) Grant No. DMR-1828019.

*Farzad.Mahfouzi@gmail.com
†Nick.Kioussis@csun.edu

[1] Sabpreet Bhatti, Rachid Sbiaa, Atsufumi Hirohata, Hideo Ohno, Shunsuke Fukami, and S. N. Piramanayagam, Spintronics based random access memory: A review, Mater. Today **20**, 530 (2017).
[2] Supriyo Datta and Biswajit Das, Electronic analog of the electrooptic modulator, Appl. Phys. Lett. **56**, 665 (1990).
[3] Pojen Chuang, Sheng-Chin Ho, L. W. Smith, F. Sfigakis, M. Pepper, Chin-Hung Chen, Ju-Chun Fan, J. P. Griffiths, and I. Farrer, All-electric all-semiconductor spin field-effect transistors, Nat. Nanotechnol. **10**, 35 (2015).
[4] Tianxiang Nan *et al.*, Acoustically actuated ultra-compact NEMS magnetoelectric antennas, Nat. Commun. **8**, 296 (2017).
[5] J. Lenz and A. S. Edelstein, Magnetic sensors and their applications, IEEE Sensors J. **6**, 631 (2006).
[6] M. I. Dyakonov and V. I. Perel, Possibility of orienting electron spins with current, JETP Lett. **13**, 467 (1971).
[7] A. Manchon and S. Zhang, Theory of nonequilibrium intrinsic spin torque in a single nanomagnet, Phys. Rev. B **78**, 212405 (2008).
[8] Ioan Mihai Miron, Kevin Garello, Gilles Gaudin, Pierre-Jean Zermatten, Marius V. Costache, Stéphane Auffret, Sébastien Bandiera, Bernard Rodmacq, Alain Schuhl, and Pietro Gambardella, Perpendicular switching of a single ferromagnetic layer induced by in-plane current injection, Nature (London) **476**, 189 (2011).
[9] Masamitsu Hayashi, Junyeon Kim, Michihiko Yamanouchi, and Hideo Ohno, Quantitative characterization of the spin-orbit torque using harmonic Hall voltage measurements, Phys. Rev. B **89**, 144425 (2014).
[10] Abhijit Ghosh, Kevin Garello, Can Onur Avci, Mihai Gabureac, and Pietro Gambardella, Interface-Enhanced Spin-Orbit Torques and Current-Induced Magnetization Switching of $\mathrm{Pd/Co/AlO}_x$ Layers, Phys. Rev. Applied **7**, 014004 (2017).
[11] Luqiao Liu, Takahiro Moriyama, D. C. Ralph, and R. A. Buhrman, Spin-Torque Ferromagnetic Resonance Induced by the Spin Hall Effect, Phys. Rev. Lett. **106**, 036601 (2011).
[12] A. M. Goncalves, I. Barsukov, Y.-J. Chen, L. Yang, J. A. Katine, and I. N. Krivorotov, Spin torque ferromagnetic resonance with magnetic field modulation, Appl. Phys. Lett. **103**, 172406 (2013).
[13] Junyeon Kim, Jaivardhan Sinha, Masamitsu Hayashi, Michihiko Yamanouchi, Shunsuke Fukami, Tetsuhiro Suzuki, Seiji Mitani, and Hideo Ohno, Layer thickness dependence of the current-induced effective field vector in Ta|CoFeB|MgO, Nat. Mater. **12**, 240 (2013).
[14] Rahul Mishra, Farzad Mahfouzi, Dushyant Kumar, Kaiming Cai, Mengji Chen, Xuepeng Qiu, Nicholas Kioussis, and Hyunsoo Yang, Electric-field control of spin accumulation

direction for spin-orbit torques, Nat. Commun. **10**, 248 (2019).
[15] Xiaoxi Huang, Shehrin Sayed, Joseph Mittelstaedt, Sandhya Susarla, Saba Karimeddiny, Lucas Caretta, Hongrui Zhang, Vladimir A. Stoica, Tanay Gosavi, Farzad Mahfouzi, Qilong Sun, Peter Ercius, Nicholas Kioussis, Sayeef Salahuddin, Daniel C. Ralph, and Ramamoorthy Ramesh, Novel spin-orbit torque generation at room temperature in an all-oxide epitaxial La0.7 Sr0.3 MnO3/SrIrO3 system, Adv. Mater. **33**, 2008269 (2021).
[16] Farzad Mahfouzi, Jaroslav Fabian, Naoto Nagaosa, and Branislav K. Nikolić, Charge pumping by magnetization dynamics in magnetic and semimagnetic tunnel junctions with interfacial Rashba or bulk extrinsic spin-orbit coupling, Phys. Rev. B **85**, 054406 (2012).
[17] Abhin Suresh, Utkarsh Bajpai, and Branislav K. Nikolić, Magnon-driven chiral charge and spin pumping and electron-magnon scattering from time-dependent quantum transport combined with classical atomistic spin dynamics, Phys. Rev. B **101**, 214412 (2020).
[18] Kapildeb Dolui, Utkarsh Bajpai, and Branislav K. Nikolić, Effective spin-mixing conductance of topological-insulator/ferromagnet and heavy-metal/ferromagnet spin-orbit-coupled interfaces: A first-principles Floquet-nonequilibrium Green function approach, Phys. Rev. Mater. **4**, 121201(R) (2020).
[19] B. Heinrich, C. Burrowes, E. Montoya, B. Kardasz, E. Girt, Y.-Y. Song, Yiyan Sun, and M. Wu, Spin Pumping at the Magnetic Insulator (YIG)/Normal Metal (Au) Interfaces, Phys. Rev. Lett. **107**, 066604 (2011).
[20] F. D. Czeschka, L. Dreher, M. S. Brandt, M. Weiler, M. Althammer, I.-M. Imort, G. Reiss, A. Thomas, W. Schoch, W. Limmer, H. Huebl, R. Gross, and S. T. B. Goennenwein, Scaling Behavior of the Spin Pumping Effect in Ferromagnet/Platinum Bilayers, Phys. Rev. Lett. **107**, 046601 (2011).
[21] Lijun Zhu, Daniel C. Ralph, and Robert A. Buhrman, Effective Spin-Mixing Conductance of Heavy-Metal-Ferromagnet Interfaces, Phys. Rev. Lett. **123**, 057203 (2019).
[22] T. Miyazaki and N. Tezuka, Giant magentic tunneling effect in Fe/Al2O3/Fe junction, J. Magn. Magn. Mater. **139**, L231 (1995).
[23] J. S. Moodera, Lisa R. Kinder, Terrilyn M. Wong, and R. Meservey, Large Magnetoresistance at Room Temperature in Ferromagnetic Thin Film Tunnel Junctions, Phys. Rev. Lett. **74**, 3273 (1995).
[24] Po-Hao Chang, Farzad Mahfouzi, Naoto Nagaosa, and Branislav K. Nikolić, Spin-Seebeck effect on the surface of a topological insulator due to nonequilibrium spin-polarization parallel to the direction of thermally driven electronic transport, Phys. Rev. B **89**, 195418 (2014).
[25] K. Uchida, S. Takahashi, K. Harii, J. Ieda, W. Koshibae, K. Ando, S. Maekawa, and E. Saitoh, Observation of the spin Seebeck effect, Nature (London) **455**, 778 (2008).
[26] D. Meier, D. Reinhardt, M. van Straaten, C. Klewe, M. Althammer, M. Schreier, S. T. B. Goennenwein, A. Gupta, M. Schmid, C. H. Back, J.-M. Schmalhorst, T. Kuschel, and G. Reiss, Longitudinal spin Seebeck effect contribution in transverse spin Seebeck effect experiments in Pt/YIG and Pt/NFO, Nat. Commun. **6**, 8211 (2015).
[27] W. Lin, K. Chen, S. Zhang, and C. L. Chien, Enhancement of Thermally Injected Spin Current through an Antiferromagnetic Insulator, Phys. Rev. Lett. **116**, 186601 (2016).
[28] M. Weiler, H. Huebl, F. S. Goerg, F. D. Czeschka, R. Gross, and S. T. B. Goennenwein, Spin Pumping with Coherent Elastic Waves, Phys. Rev. Lett. **108**, 176601 (2012).
[29] Hiroki Hayashi and Kazuya Ando, Spin Pumping Driven by Magnon Polarons, Phys. Rev. Lett. **121**, 237202 (2018).
[30] Jérôme Hurst, Paul-Antoine Hervieux, and Giovanni Manfredi, Spin current generation by ultrafast laser pulses in ferromagnetic nickel films, Phys. Rev. B **97**, 014424 (2018).
[31] Gyung-Min Choi, Byoung-Chul Min, Kyung-Jin Lee, and David G. Cahill, Spin current generated by thermally driven ultrafast demagnetization, Nat. Commun. **5**, 4334 (2014).
[32] Takuya Kawada, Masashi Kawaguchi, Takumi Funato, Hiroshi Kohno, and Masamitsu Hayashi, Acoustic spin Hall effect in strong spin-orbit metals, Sci. Adv. **7**, eabd9697 (2021).
[33] G. Sundaram and Q. Niu, Wave-packet dynamics in slowly perturbed crystals: Gradient corrections and berry-phase effects, Phys. Rev. B **59**, 14915 (1999).
[34] S. Chaudhary, M. Endres, and G. Refael, Berry electrodynamics: Anomalous drift and pumping from a time-dependent berry connection, Phys. Rev. B **98**, 064310 (2018).
[35] C. L. Romano, G. E. Marques, L. Sanz, and A. M. Alcalde, Phonon modulation of the spin-orbit interaction as a spin relaxation mechanism in quantum dots, Phys. Rev. B **77**, 033301 (2008).
[36] Yu-Ling Hsueh, Holger Büch, Yaohua Tan, Yu Wang, Lloyd C. L. Hollenberg, Gerhard Klimeck, Michelle Y. Simmons, and Rajib Rahman, Spin-Lattice Relaxation Times of Single Donors and Donor Clusters in Silicon, Phys. Rev. Lett. **113**, 246406 (2014).
[37] Timothy B. Boykin, Gerhard Klimeck, R. Chris Bowen, and Fabiano Oyafuso, Diagonal parameter shifts due to nearest-neighbor displacements in empirical tight-binding theory, Phys. Rev. B **66**, 125207 (2002).
[38] Farzad Mahfouzi, Jinwoong Kim, and Nicholas Kioussis, Intrinsic damping phenomena from quantum to classical magnets: An *ab initio* study of Gilbert damping in a Pt/Co bilayer, Phys. Rev. B **96**, 214421 (2017).
[39] Jiawei Zhou, Bolin Liao, Bo Qiu, Samuel Huberman, Keivan Esfarjani, Mildred S. Dresselhaus, and Gang Chen, *Ab initio* optimization of phonon drag effect for lower-temperature thermoelectric energy conversion, Proc. Natl. Acad. Sci. U.S.A. **112**, 14777 (2015).
[40] Farzad Mahfouzi and Nicholas Kioussis, Current-induced damping of nanosized quantum moments in the presence of spin-orbit interaction, Phys. Rev. B **95**, 184417 (2017).
[41] See Supplemental Material at http://link.aps.org/supplemental/10.1103/PhysRevLett.128.215902 for complementary results and discussions, which contains Refs. [42,43].
[42] P. J. Leek, M. R. Buitelaar, V. I. Talyanskii, C. G. Smith, D. Anderson, G. A. C. Jones, J. Wei, and D. H. Cobden, Charge Pumping in Carbon Nanotubes, Phys. Rev. Lett. **95**, 256802 (2005).
[43] G. Y. Guo, S. Murakami, T.-W. Chen, and N. Nagaosa Intrinsic Spin Hall Effect in Platinum: First-Principles Calculations, Phys. Rev. Lett. **100**, 096401 (2008).

[44] D. J. Thouless, Quantization of particle transport, Phys. Rev. B **27**, 6083 (1983).
[45] T. Ozaki, Variationally optimized atomic orbitals for large-scale electronic structures, Phys. Rev. B **67**, 155108 (2003).
[46] T. Ozaki and H. Kino, Numerical atomic basis orbitals from H to Kr, Phys. Rev. B **69**, 195113 (2004).
[47] T. Ozaki and H. Kino, Efficient projector expansion for the *ab initio* LCAO method, Phys. Rev. B **72**, 045121 (2005).
[48] Farzad Mahfouzi, Rahul Mishra, Po-Hao Chang, Hyunsoo Yang, and Nicholas Kioussis, Microscopic origin of spin-orbit torque in ferromagnetic heterostructures: A first-principles approach, Phys. Rev. B **101**, 060405(R) (2020).
[49] F. Mahfouzi and N. Kioussis, First-principles study of the angular dependence of the spin-orbit torque in Pt/Co and Pd/Co bilayers, Phys. Rev. B **97**, 224426 (2018).
[50] N. Troullier and J. L. Martins, Efficient pseudopotentials for plane-wave calculations, Phys. Rev. B **43**, 1993 (1991).
[51] D. M. Ceperley and B. J. Alder, Ground State of the Electron Gas by a Stochastic Method, Phys. Rev. Lett. **45**, 566 (1980).
[52] John P. Perdew and Yue Wang, Accurate and simple analytic representation of the electron-gas correlation energy, Phys. Rev. B **45**, 13244 (1992).
[53] Farzad Mahfouzi, Gregory P. Carman, and Nicholas Kioussis, Magnetoelastic and magnetostrictive properties of Co2XAl Heusler compounds, Phys. Rev. B **102**, 094401 (2020).
[54] Ken Nakano, Akihiro Torii, Kazuhiro Hane, and Shigeru Okuma, Visualization of high-frequency surface acoustic wave propagation using stroboscopic phase- shift interferometry, *SPIE Proceedings Vol. 3225, Microlithography and Metrology in Micromachining III* (SPIE International Society for Optical Engineering, Bellingham, WA, 1997).
[55] Junren Shi, Ping Zhang, Di Xiao, and Qian Niu, Proper Definition of Spin Current in Spin-Orbit Coupled Systems, Phys. Rev. Lett. **96**, 076604 (2006).
[56] Ping Zhang, Zhigang Wang, Junren Shi, Di Xiao, and Qian Niu, Theory of conserved spin current and its application to a two-dimensional hole gas, Phys. Rev. B **77**, 075304 (2008).
[57] Domenico Monaco and Lara Ulcakar, Spin Hall conductivity in insulators with nonconserved spin, Phys. Rev. B **102**, 125138 (2020).
[58] Gordon Baym and Leo P. Kadanoff, Conservation laws and correlation functions, Phys. Rev. **124**, 287 (1961).